Temporal Structures in Positron Spectra and Charge-Sign Effects in Galactic Cosmic Rays

M. Aguilar,[29] G. Ambrosi,[35] H. Anderson,[10] L. Arruda,[27] N. Attig,[24] C. Bagwell,[10] F. Barao,[27] M. Barbanera,[35] L. Barrin,[14] A. Bartoloni,[39] R. Battiston,[46,47] N. Belyaev,[10] J. Berdugo,[29] B. Bertucci,[35,36] V. Bindi,[20] K. Bollweg,[21] J. Bolster,[10] M. Borchiellini,[17] B. Borgia,[39,40] M. J. Boschini,[31] M. Bourquin,[15] J. Burger,[10] W. J. Burger,[46] X. D. Cai,[10] M. Capell,[10] J. Casaus,[29] G. Castellini,[13] F. Cervelli,[37] Y. H. Chang,[44] G. M. Chen,[6,7] G. R. Chen,[23] H. Chen,[19] H. S. Chen,[6,7] Y. Chen,[15,23] L. Cheng,[23] H. Y. Chou,[44] S. Chouridou,[1] V. Choutko,[10] C. H. Chung,[1] C. Clark,[10,21] G. Coignet,[3] C. Consolandi,[20] A. Contin,[8,9] C. Corti,[20] Z. Cui,[22,23] K. Dadzie,[10] F. D'Angelo,[9,8] A. Dass,[46,47] C. Delgado,[29] S. Della Torre,[31] M. B. Demirköz,[2] L. Derome,[16] S. Di Falco,[37] V. Di Felice,[41] C. Díaz,[29] F. Dimiccoli,[46] P. von Doetinchem,[20] F. Dong,[33] F. Donnini,[35] M. Duranti,[35] A. Egorov,[10] A. Eline,[10] F. Faldi,[35,36] J. Feng,[18] E. Fiandrini,[35,36] P. Fisher,[10] V. Formato,[41] C. Gámez,[29] R. J. García-López,[26] C. Gargiulo,[14] H. Gast,[1] M. Gervasi,[31,32] F. Giovacchini,[29] D. M. Gómez-Coral,[30] J. Gong,[33] C. Goy,[3] D. Grandi,[31,32] M. Graziani,[35,36] A. N. Guracho,[39] S. Haino,[44] K. C. Han,[28] R. K. Hashmani,[2] Z. H. He,[18] B. Heber,[25] T. H. Hsieh,[10] J. Y. Hu,[6,7] B. W. Huang,[19] M. Ionica,[35] M. Incagli,[37] Yi Jia,[10] H. Jinchi,[28] G. Karagöz,[2] S. Khan,[15] B. Khiali,[41] Th. Kirn,[1] A. P. Klipfel,[10] O. Kounina,[10] A. Kounine,[10] V. Koutsenko,[10] D. Krasnopevtsev,[10] A. Kuhlman,[20] A. Kulemzin,[10] G. La Vacca,[31,32] E. Laudi,[14] G. Laurenti,[8] G. LaVecchia,[10] I. Lazzizzera,[46,47] H. T. Lee,[43] S. C. Lee,[44] H. L. Li,[23] J. Q. Li,[33] M. Li,[15] M. Li,[22] Q. Li,[33] Q. Li,[22] Q. Y. Li,[23] S. Li,[1] S. L. Li,[6,7] J. H. Li,[22] Z. H. Li,[6,7] J. Liang,[22] M. J. Liang,[6,7] C. H. Lin,[44] T. Lippert,[24] J. H. Liu,[5] S. Q. Lu,[44] Y. S. Lu,[6] K. Luebelsmeyer,[1] J. Z. Luo,[33] S. D. Luo,[19] Xi Luo,[23] C. Mañá,[29] J. Marín,[29] J. Marquardt,[25] T. Martin,[10,21] G. Martínez,[29] N. Masi,[8] D. Maurin,[16] T. Medvedeva,[10] A. Menchaca-Rocha,[30] Q. Meng,[33] M. Molero,[26] P. Mott,[10,21] L. Mussolin,[35,36] Y. Najafi Jozani,[1] J. Negrete,[20] R. Nicolaidis,[47,46] N. Nikonov,[20] F. Nozzoli,[46] J. Ocampo-Peleteiro,[29] A. Oliva,[8] M. Orcinha,[27] M. A. Ottupara,[23] M. Palermo,[20] F. Palmonari,[8,9] M. Paniccia,[15] A. Pashnin,[10] M. Pauluzzi,[35,36] S. Pensotti,[31,32] V. Plyaskin,[10] S. Poluianov,[34] X. Qin,[10] Z. Y. Qu,[23] L. Quadrani,[8,9] P. G. Rancoita,[31] D. Rapin,[15] A. Reina Conde,[8] E. Robyn,[15] I. Rodríguez-García,[29] L. Romaneehsen,[25] F. Rossi,[47,46] A. Rozhkov,[10] D. Rozza,[31] R. Sagdeev,[11] E. Savin,[9,8] S. Schael,[1] A. Schultz von Dratzig,[1] G. Schwering,[1] E. S. Seo,[12] B. S. Shan,[4] T. Siedenburg,[1] G. Silvestre,[35] J. W. Song,[22] X. J. Song,[23] R. Sonnabend,[1] L. Strigari,[39,*] T. Su,[23] Q. Sun,[22] Z. T. Sun,[6,7] M. Tacconi,[31,32] X. W. Tang,[6] Z. C. Tang,[6] J. Tian,[41] Y. Tian,[19] Samuel C. C. Ting,[10,14] S. M. Ting,[10] N. Tomassetti,[35,36] J. Torsti,[48] T. Urban,[10,21] I. Usoskin,[34] V. Vagelli,[38,35] R. Vainio,[48] M. Valencia-Otero,[45] E. Valente,[39,40] E. Valtonen,[48] M. Vázquez Acosta,[26] M. Vecchi,[17] M. Velasco,[29] J. P. Vialle,[3] C. X. Wang,[22] L. Wang,[5] L. Q. Wang,[22] N. H. Wang,[22] Q. L. Wang,[5] S. Wang,[20] X. Wang,[10] Yu Wang,[22] Z. M. Wang,[23] J. Wei,[15,23] Z. L. Weng,[10] H. Wu,[33] Y. Wu,[23] J. N. Xiao,[19] R. Q. Xiong,[33] X. Z. Xiong,[19] W. Xu,[22,23] Q. Yan,[10] H. T. Yang,[6,7] Y. Yang,[42] A. Yelland,[10] H. Yi,[33] Y. H. You,[6,7] Y. M. Yu,[10] Z. Q. Yu,[6] C. Zhang,[6] F. Zhang,[6] F. Z. Zhang,[6,7] J. Zhang,[22] J. H. Zhang,[33] Z. Zhang,[10] F. Zhao,[6,7] C. Zheng,[23] Z. M. Zheng,[4] H. L. Zhuang,[6] V. Zhukov,[1] A. Zichichi,[8,9] and P. Zuccon[46,47]

(AMS Collaboration)

[1]*I. Physics Institute and JARA-FAME, RWTH Aachen University, 52056 Aachen, Germany*
[2]*Department of Physics, Middle East Technical University (METU), 06800 Ankara, Türkiye*
[3]*Université Grenoble Alpes, Université Savoie Mont Blanc, CNRS, LAPP-IN2P3, 74000 Annecy, France*
[4]*Beihang University (BUAA), Beijing 100191, China*
[5]*Institute of Electrical Engineering (IEE), Chinese Academy of Sciences, Beijing 100190, China*
[6]*Institute of High Energy Physics (IHEP), Chinese Academy of Sciences, Beijing 100049, China*
[7]*University of Chinese Academy of Sciences (UCAS), Beijing 100049, China*
[8]*INFN Sezione di Bologna, 40126 Bologna, Italy*
[9]*Università di Bologna, 40126 Bologna, Italy*
[10]*Massachusetts Institute of Technology (MIT), Cambridge, Massachusetts 02139, USA*
[11]*East-West Center for Space Science, University of Maryland, College Park, Maryland 20742, USA*
[12]*IPST, University of Maryland, College Park, Maryland 20742, USA*
[13]*CNR-IROE, 50125 Firenze, Italy*
[14]*European Organization for Nuclear Research (CERN), 1211 Geneva 23, Switzerland*
[15]*DPNC, Université de Genève, 1211 Genève 4, Switzerland*
[16]*Université Grenoble Alpes, CNRS, Grenoble INP, LPSC-IN2P3, 38000 Grenoble, France*

[17]Kapteyn Astronomical Institute, University of Groningen, P.O. Box 800, 9700 AV Groningen, Netherlands
[18]Sun Yat-Sen University (SYSU), Guangzhou 510275, China
[19]Zhejiang University (ZJU), Hangzhou 310058, China
[20]Physics and Astronomy Department, University of Hawaii, Honolulu, Hawaii 96822, USA
[21]National Aeronautics and Space Administration Johnson Space Center (JSC), Houston, Texas 77058, USA
[22]Shandong University (SDU), Jinan, Shandong 250100, China
[23]Shandong Institute of Advanced Technology (SDIAT), Jinan, Shandong 250100, China
[24]Jülich Supercomputing Centre and JARA-FAME, Research Centre Jülich, 52425 Jülich, Germany
[25]Institut für Experimentelle und Angewandte Physik, Christian-Alberts-Universität zu Kiel, 24118 Kiel, Germany
[26]Instituto de Astrofísica de Canarias (IAC), 38205 La Laguna, and Departamento de Astrofísica, Universidad de La Laguna, 38206 La Laguna, Tenerife, Spain
[27]Laboratório de Instrumentação e Física Experimental de Partículas (LIP), 1649-003 Lisboa, Portugal
[28]National Chung-Shan Institute of Science and Technology (NCSIST), Longtan, Tao Yuan 32546, Taiwan
[29]Centro de Investigaciones Energéticas, Medioambientales y Tecnológicas (CIEMAT), 28040 Madrid, Spain
[30]Instituto de Física, Universidad Nacional Autónoma de México (UNAM), Ciudad de México, 01000 Mexico
[31]INFN Sezione di Milano-Bicocca, 20126 Milano, Italy
[32]Università di Milano-Bicocca, 20126 Milano, Italy
[33]Southeast University (SEU), Nanjing 210096, China
[34]Sodankylä Geophysical Observatory and Space Physics and Astronomy Research Unit, University of Oulu, 90014 Oulu, Finland
[35]INFN Sezione di Perugia, 06100 Perugia, Italy
[36]Università di Perugia, 06100 Perugia, Italy
[37]INFN Sezione di Pisa, 56100 Pisa, Italy
[38]Agenzia Spaziale Italiana (ASI), 00133 Roma, Italy
[39]INFN Sezione di Roma 1, 00185 Roma, Italy
[40]Università di Roma La Sapienza, 00185 Roma, Italy
[41]INFN Sezione di Roma Tor Vergata, 00133 Roma, Italy
[42]National Cheng Kung University, Tainan 70101, Taiwan
[43]Academia Sinica Grid Center (ASGC), Nankang, Taipei 11529, Taiwan
[44]Institute of Physics, Academia Sinica, Nankang, Taipei 11529, Taiwan
[45]Physics Department and Center for High Energy and High Field Physics, National Central University (NCU), Tao Yuan 32054, Taiwan
[46]INFN TIFPA, 38123 Trento, Italy
[47]Università di Trento, 38123 Trento, Italy
[48]Space Research Laboratory, Department of Physics and Astronomy, University of Turku, 20014 Turku, Finland

(Received 23 July 2023; revised 26 August 2023; accepted 1 September 2023; published 12 October 2023)

We present the precision measurements of 11 years of daily cosmic positron fluxes in the rigidity range from 1.00 to 41.9 GV based on 3.4×10^6 positrons collected with the Alpha Magnetic Spectrometer (AMS) aboard the International Space Station. The positron fluxes show distinctly different time variations from the electron fluxes at short and long timescales. A hysteresis between the electron fluxes and the positron fluxes is observed with a significance greater than 5σ at rigidities below 8.5 GV. On the contrary, the positron fluxes and the proton fluxes show similar time variation. Remarkably, we found that positron fluxes are modulated more than proton fluxes with a significance greater than 5σ for rigidities below 7 GV. These continuous daily positron fluxes, together with AMS daily electron, proton, and helium fluxes over an 11-year solar cycle, provide unique input to the understanding of both the charge-sign and mass dependencies of cosmic rays in the heliosphere.

DOI: 10.1103/PhysRevLett.131.151002

Knowledge of light cosmic-ray antimatter species, such as positrons, antiprotons, and antideuterons, is crucial for the understanding of phenomena in the cosmos [1–3], such as the nature of dark matter. The yield of these particles is small. The study of cosmic antimatter with a precise magnetic spectrometer enables us to separate it from the overwhelming background of matter.

The measurements of the cosmic positron flux with the Alpha Magnetic Spectrometer (AMS) on the International Space Station (ISS) [4,5] and earlier measurements [6] have generated widespread interest and discussions of the observed excess of high-energy positrons. The explanations of these results included three classes of models: annihilation of dark matter particles [1], acceleration of positrons to high energies in astrophysical objects [2], such as pulsars, and production of high-energy positrons in the interactions of cosmic-ray nuclei with interstellar gas [3]. Models describing these phenomena can be compared to data only when time-dependent effects in the heliosphere are well understood.

The fluxes of interstellar charged cosmic rays are thought to be stable on the timescale of decades [7–10]. Time-dependent structures in the energy spectra of galactic cosmic rays are expected from the solar modulation [11] only when they enter the heliosphere. Solar modulation involves convective, diffusive, particle drift, and adiabatic energy change processes. Only particle drift induces a dependence of solar modulation on the particle charge sign [12]. Since positrons and electrons differ only in charge sign, positrons and protons share the same charge sign with different masses, and helium provides different information on both charge and mass, their simultaneous measurement over an 11-year solar cycle offers a unique way to study charge-sign- and mass-dependent solar modulation effects at different timescales.

Previously, AMS has reported the time dependence per Bartels rotation (BR: 27 days) of positron fluxes and separately electron fluxes over six years [13]. AMS has recently reported short-term variations on the scale of days to months and long-term variations on the scale of years in the daily cosmic-ray electron [14], proton [15], and helium [16] fluxes over 11 years.

This Letter reports the first daily positron flux measurement. In the past, PAMELA has measured three-month average positron-to-electron flux ratio variation over nine years [17].

In this Letter, we present the daily positron fluxes spanning 11 years over a rigidity range from 1.00 to 41.9 GV. These data cover the major portion of solar cycle 24, which includes the polarity reversal of the solar magnetic field in the year 2013 [18], and the first part of solar cycle 25. Therefore, both the charge-sign- and mass-dependent effects at different solar conditions are studied by comparing the daily positron, daily electron [14], and daily proton [15] fluxes measured simultaneously over an 11-year period. These data provide unique and accurate input to the understanding of the transport processes of charged cosmic rays inside the heliosphere.

Detector.—The layout and description of the AMS detector are presented in Refs. [19,20] and shown in Fig. S1 in Supplemental Material [21]. The key elements used in this measurement are the permanent magnet [22], the silicon tracker [23–25], the transition radiation detector (TRD) [26], the four planes of time of flight (TOF) scintillation counters [27], and the electromagnetic calorimeter (ECAL) [28,29]. Further information on the AMS layout, performance, trigger, and the Monte Carlo simulation [30] is detailed in Supplemental Material [21].

Event selection.—AMS has collected 1.9×10^{11} cosmic-ray events. In the rigidity range from 1.00 to 41.9 GV, we select positron samples using the combined information of TRD, TOF, inner tracker, and ECAL. The details of the event selection, including the geomagnetic cutoff [31–33] and backgrounds, are contained in Supplemental Material [21] and in Refs. [5,19]. After selection and background subtraction, we obtained 3.4×10^6 positrons.

Data analysis.—The daily isotropic flux in the ith rigidity bin $(R_i, R_i + \Delta R_i)$ and jth day is given by

$$\Phi_i^j = \frac{N_i^j}{A_i^j(1+\delta_i^j)\epsilon_i^j T_i^j \Delta R_i}, \tag{1}$$

where N_i^j is the number of events corrected for small background (∼1%) and bin-to-bin migration using the unfolding procedure described in Ref. [34], A_i^j is the effective acceptance calculated from the Monte Carlo simulation including geometric acceptance, event selection efficiencies, and interactions of positrons in the AMS materials, δ_i^j is the small correction to the acceptance due to the difference in selection efficiencies between data and Monte Carlo simulation, ϵ_i^j is the trigger efficiency, and T_i^j is the daily collection time (see Supplemental Material [21] for details). The positron flux is measured in 12 rigidity bins from 1.00 to 41.9 GV. The binning is similar to that in our electron [14] and proton [15] daily flux measurements.

The small corrections δ_i^j are estimated by comparing the efficiencies in data and Monte Carlo simulation of every selection cut using information from the detectors unrelated to that cut [5]. The δ_i^j are found to have a small rigidity dependence smoothly varying from −5% at 1 GV, to −1% from 2 to 6 GV, to −5% at 41.9 GV.

The trigger efficiency ϵ_i^j is 100% above 3 GV, decreasing to 83% at 1 GV [19], and is stable over time within errors.

Extensive studies were made of both the time-dependent and time-independent systematic errors. These errors include the uncertainties in background subtraction, the trigger efficiency, the geomagnetic cutoff, the small correction to the acceptance calculation (δ_i^j), the unfolding, and the absolute energy scale.

The uncertainty associated with the proton background subtraction includes two parts: the event selection and the statistical fluctuation of the TRD estimator Λ_{TRD} used to differentiate $e^{\pm}$ from p [5]. These two errors are found to be independent and are added in quadrature. The systematic

error due to proton background subtraction is found to be $< 0.5\%$ of the flux over the entire rigidity range.

The amount of charge confusion is well reproduced by the Monte Carlo simulation [5]. The associated systematic error on the fluxes is negligible ($< 0.1\%$) over the entire rigidity range.

The time-dependent systematic error on the positron fluxes associated with the trigger efficiency measurement is $<1\%$ below 3 GV and negligible above 3 GV.

The geomagnetic cutoff is calculated as described in Supplemental Material [21], and the resulting systematic error on the fluxes is less than 2% at 1 GV and negligible ($< 0.4\%$) above 2 GV.

The systematic error from the correction δ_i^j on the fluxes is time dependent and amounts to $< 1.5\%$ over the entire rigidity range.

The systematic error associated with the unfolding includes time-dependent and time-independent errors. The time-independent error is estimated to be 1% of the flux at 1.00 GV and decreases to $< 0.2\%$ above 10 GV [5]. The daily flux spectral shape variation leads to an additional time-dependent uncertainty in the unfolding procedure, which is $< 1.0\%$ at 1 GV and negligible ($< 0.2\%$) above 5 GV.

The uncertainty on the absolute energy scale [29] is 2.7% at 1 GV, decreasing to 2.0% in the range 2–41.9 GV and is found to be stable at the level of 0.2% for all energies. The energy scale error is treated as an uncertainty of the bin boundaries.

The time-dependent contributions to the systematic error from the background subtraction, the trigger efficiency, the event selection efficiencies, and the unfolding are evaluated independently each day and are found to be uncorrelated. They are added in quadrature to derive a time-dependent systematic error, which is 1.5% at 1 GV and $\sim$1% above 2 GV for all days.

The daily total systematic error is obtained by adding in quadrature the individual contributions of the time-independent systematic errors discussed above and the time-dependent systematic errors. At 1 GV, it is less than 3%, and above 3 GV, it is $\sim$1.5% for all days.

Most importantly, independent analyses were performed on the same data sample by three different study groups. The results of those analyses are consistent with this Letter.

Results.—The daily positron fluxes, including statistical errors, time-dependent systematic errors, and total systematic errors are tabulated in Tables S1–S3268 in Supplemental Material [21] and in a machine-readable form [35] as functions of the rigidity at the top of the AMS detector. These data are in agreement with our earlier 27-day results [13] in the overlapping time period.

Figure 1 shows the daily positron flux Φ_{e^+} in the rigidity range from 1.00 to 1.71 GV, measured from May 20, 2011 to November 2, 2021, together with (a) the daily electron flux Φ_{e^-} and (b) the daily proton flux Φ_p, both measured by

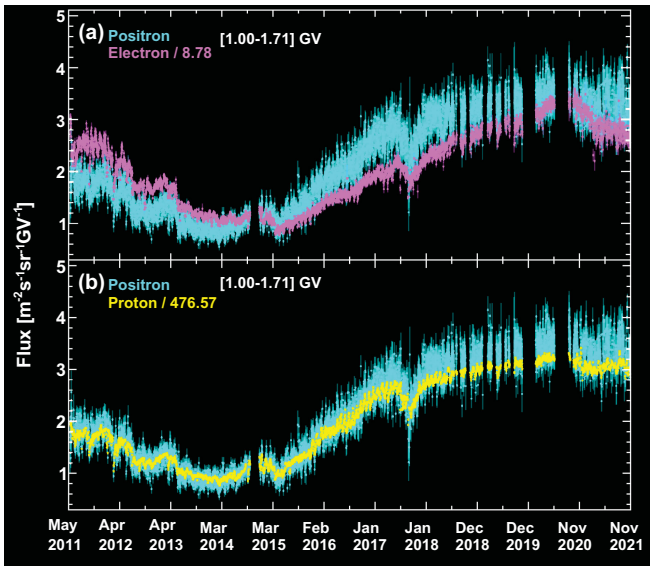

FIG. 1. The daily positron fluxes (light blue points) measured over the entire period for the rigidity range from 1.00 to 1.71 GV together with (a) the daily electron fluxes (magenta points) and (b) the daily proton fluxes (yellow points). Days with solar energetic particle events are excluded from Φ_p. The gaps in the fluxes are due to detector studies and upgrades. Electron and proton fluxes are divided by different scale factors as indicated. The scale factors are chosen such that the positron, electron, and proton fluxes are at the same magnitude on average during 2014 and 2015. As seen, the positron fluxes exhibit short-term variations on the scale of days to months and long-term variations on the scale of years. The long-term evolution of positron and electron fluxes is clearly different. On the contrary, positron and proton fluxes present a similar behavior over time.

AMS in the same rigidity range and time period [14,15]. In these and subsequent figures, the error bars on the fluxes are the quadratic sum of the statistical and time-dependent systematic errors. As seen, Φ_{e^+} exhibits short-term variations on the scale of days to months and long-term variations on the scale of years. Figure 1(a) shows that the long-term evolution of positron and electron fluxes is clearly different. On the contrary, Fig. 1(b) shows that positron and proton fluxes present a similar behavior over time. The detailed comparison will be presented below.

The time evolution of Φ_{e^+} and Φ_{e^-} is presented in Fig. S2 in Supplemental Material [21] for four rigidity bins from 1.00 to 41.9 GV. Φ_{e^+} and Φ_{e^-} are shown averaged over 3 days. At low rigidities, below $\sim$8.5 GV, Φ_{e^+} and Φ_{e^-} present a different behavior over time. In 2011–2014, Φ_{e^+} decreases more slowly with time than Φ_{e^-}. Then, from 2014 to 2017, both fluxes start rising, but Φ_{e^+} rises faster than Φ_{e^-}. From 2017 to 2020, Φ_{e^+} rises more slowly than Φ_{e^-}. In 2020, both fluxes reach their maxima. From mid-2020 to 2021, both fluxes decrease and Φ_{e^+} decreases more slowly than Φ_{e^-}. As seen from Figs. S2(a)–S2(d), the difference between the time evolution of Φ_{e^+} and Φ_{e^-}

decreases with increasing rigidity, becoming negligible in the rigidity range [22.8–41.9] GV; see Fig. S2(d).

The comparison of the time evolution of 3-day averaged Φ_{e^+} and Φ_p in the entire period is shown in Fig. S3 in Supplemental Material [21] for the same four rigidity bins from 1.00 to 41.9 GV. As seen, both fluxes present a similar behavior over time, and at low rigidity [Figs. S3(a) and S3(b)] Φ_{e^+} exhibits a larger variation than Φ_p. At higher rigidities [Fig. S3(c)], the difference in their respective time evolution decreases and becomes negligible in the rigidity range [22.8–41.9] GV [Fig. S3(d)].

Short-term variations in Φ_{e^+} are shown in Fig. S4 in Supplemental Material [21] in the rigidity range from 1.00 to 2.97 GV, together with Φ_{e^-} and Φ_p, measured from January 1, 2016 to January 1, 2017. Φ_{e^+}, Φ_{e^-}, and Φ_p are shown averaged over 3 days. As seen, Φ_{e^+} shows time variations that are different from those observed in Φ_{e^-}. On the contrary, Φ_{e^+} and Φ_p exhibit similar time variations.

These results show that the time evolution of Φ_{e^+} is similar to Φ_p and distinctly different from Φ_{e^-} in short term and long term, indicating a clear charge-sign dependence in the solar modulation for positrons and electrons.

To study the recurrent variations in the daily Φ_{e^+}, a wavelet time-frequency technique [36] was used to locate the time intervals where the periodic structures emerge. The details on the wavelet analysis are described in Supplemental Material [21]. Φ_{e^+} for the rigidity interval from 1.00 to 2.97 GV in each year (2011–2021 defined in Table SA in Supplemental Material [21]), together with their time-averaged power spectra and 95% confidence levels, are shown in Figs. S5–S15 in Supplemental Material [21]. Significant values of the normalized power around 27 days are observed in the second half of 2015, the first half of 2016, the first half of 2017, and the first half of 2018. The analysis of Φ_p presented in Ref. [15] also showed significant 27-day periodicity in these four time intervals.

The long-term variations on the scale of years are related to the 11- and 22-year cycles of the solar magnetic field [11]. To investigate the difference in the modulation of Φ_{e^+}, Φ_{e^-} and Φ_p, Fig. 2 shows Φ_{e^-} and Φ_p as functions of Φ_{e^+} in the rigidity range from 1.00 to 1.71 GV. For Figs. 2(a) and 2(b), the data points correspond to fluxes averaged over 3 days. For Figs. 2(c) and 2(d), Φ_{e^+}, Φ_{e^-}, and Φ_p are calculated with a moving average of 14 BRs and a step of 3 days. Different colors indicate different years from 2011 to 2021. In Fig. 2(c), a hysteresis between Φ_{e^+} and Φ_{e^-} is clearly observed. From 2011 to 2018, at a given Φ_{e^-}, Φ_{e^+} shows two distinct branches with time, one before

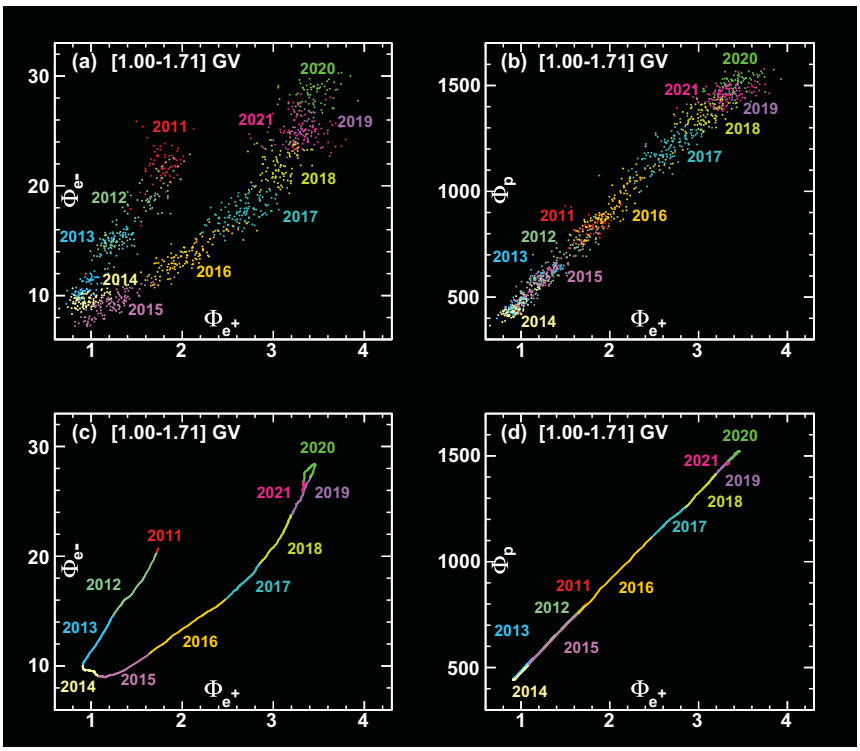

FIG. 2. In the rigidity range from 1.00 to 1.71 GV, (a),(c) electron flux Φ_{e^-} versus positron flux Φ_{e^+} and (b),(d) proton flux Φ_p versus positron flux Φ_{e^+}. For (a),(b), the data points correspond to fluxes averaged over 3 days. For (c),(d), Φ_{e^-}, Φ_p, and Φ_{e^+} are calculated with a moving average of 14 BRs and a step of 3 days. Fluxes are in units of [m^{-2} sr^{-1} s^{-1} GV^{-1}]. Different colors indicate different years.

2014–2015 and one after. Around 2017, the hysteresis curve changes such that in 2018–2020 it is nearly parallel to that in 2011–2013. Similar behavior is observed in the Φ_{e^-} to Φ_p correlation (see Fig. 3 in Ref. [14]). On the contrary, as seen from Fig. 2(d), there is a nearly linear correlation between Φ_{e^+} and Φ_p in the entire time period. Figure 2 also shows that the three fluxes Φ_{e^+}, Φ_{e^-}, and Φ_p peak in 2020, after which the fluxes start to trace their earlier behavior (2018–2020) backwards.

The significance of the hysteresis between Φ_{e^+} and Φ_{e^-} has been evaluated following an analysis similar to that described in Ref. [14] (see Figs. S16 and S17 in Supplemental Material [21] for details). The significance is greater than 10σ at the rigidity bin [1.00–1.71] GV and greater than 5σ for each rigidity bin below 8.48 GV.

To probe structures in the hysteresis, the moving averages of the Φ_{e^+} and Φ_{e^-} are calculated with a finer time window, and the result is shown in Fig. 3 for the rigidity range from 1.00 to 1.71 GV. Figure 3(a) shows the daily Φ_{e^+} and Φ_{e^-} as a function of time over the entire period. The dashed lines I, II, and III indicate the location of sharp dips in Φ_{e^+} and Φ_{e^-}, and the colored bands IV and V mark the time intervals around the dips in 2015 and 2017. The moving average of Φ_{e^+} and Φ_{e^-} with a time window of 2 BRs and a step of 1 day is shown in Fig. 3(b). The detailed behavior around dips IV and V is shown in Fig. S18 in Supplemental Material [21].

To analyze the significance of the structures in the positron-electron hysteresis, we study the difference of Φ_{e^-} at the same Φ_{e^+}, one in the first half and one in the second half of each region, IV and V (see Fig. S18 and the description in Supplemental Material [21] for details). The significance at the rigidity interval [1.00–1.71] GV for region IV is $> 10\sigma$ [see Fig. S18(c)] and for region V is 4σ [see Fig. S18(d)].

The structures in the observed hysteresis in 2015 and 2017 between Φ_{e^+} and Φ_{e^-} are similar to those observed between Φ_{e^-} and Φ_p [14] and are likely caused by two series of interplanetary coronal mass ejections [37]. The clear deviation, regions IV and V in Fig. 3 [see also Figs. S18(b)–S18(d)], from the long-term trend implies a charge-sign-dependent modulation during those solar transients on the timescale of several Bartels rotations.

Figure 1(b) [see also Fig. S19(a) in Supplemental Material [21]) shows the daily Φ_{e^+} and Φ_p as a function of time over the entire period for the rigidity range from 1.00 to 1.71 GV. Φ_p versus Φ_{e^+}, calculated with a moving average of 2 BRs and a step of 1 day, is shown in Figs. S19(b)–S19(d) in Supplemental Material [21]. As seen, a nearly linear correlation between positron and proton fluxes is observed, and no significant structures are found.

To compare the daily time variations of Φ_{e^+} and Φ_p, we fit a linear relation between the relative variations of the fluxes for the ith rigidity bin $(R_i, R_i + \Delta R_i)$ as

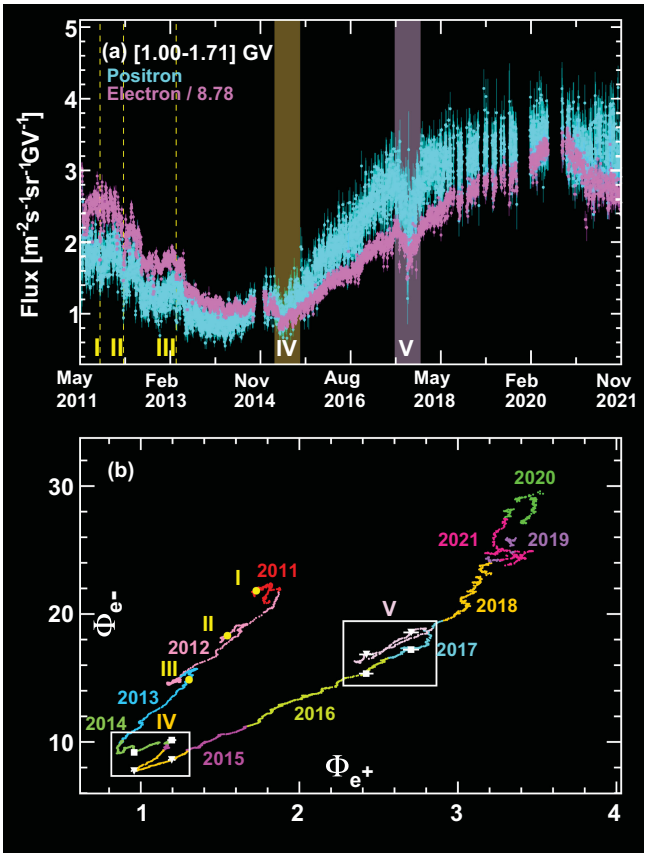

FIG. 3. (a) The daily positron fluxes (light blue points) together with the daily electron fluxes (magenta points), measured for the rigidity interval from 1.00 to 1.71 GV over the entire period. For display purposes, the electron fluxes are divided by a scale factor such that Φ_{e^+} and Φ_{e^-} are at the same magnitude on average during 2014 and 2015. Dashed lines I, II, and III indicate the location of sharp dips in the positron and electron fluxes, and colored bands IV and V mark the time intervals around the dips in 2015 and 2017. (b) Electron flux Φ_{e^-} versus positron flux Φ_{e^+}, both calculated with a moving average of 2 BRs and a step of 1 day. Fluxes are in units of [m^{-2} sr^{-1} s^{-1} GV^{-1}]. Different colors indicate different years from 2011 to 2021. The locations of I, II, and III correspond to the flux dips in (a). Time intervals IV and V around the dips in 2015 and 2017 in (a) are indicated by white boxes. White squares and white triangles mark the two pairs of time intervals used to evaluate the significance of the structures in the hysteresis.

$$\frac{\Phi^i_{e^+} - \langle \Phi^i_{e^+} \rangle}{\langle \Phi^i_{e^+} \rangle} = k^i \cdot \frac{\Phi^i_p - \langle \Phi^i_p \rangle}{\langle \Phi^i_p \rangle}, \tag{2}$$

where k^i is the slope of the linear dependence for that bin and $\langle \Phi^i_{e^+} \rangle$ and $\langle \Phi^i_p \rangle$ are the positron and proton fluxes in the ith rigidity bin averaged over the entire period, respectively.

Examples of fits of the daily positron and the daily proton fluxes to Eq. (2) are shown in Fig. S20 in Supplemental Material [21] for six consecutive rigidity

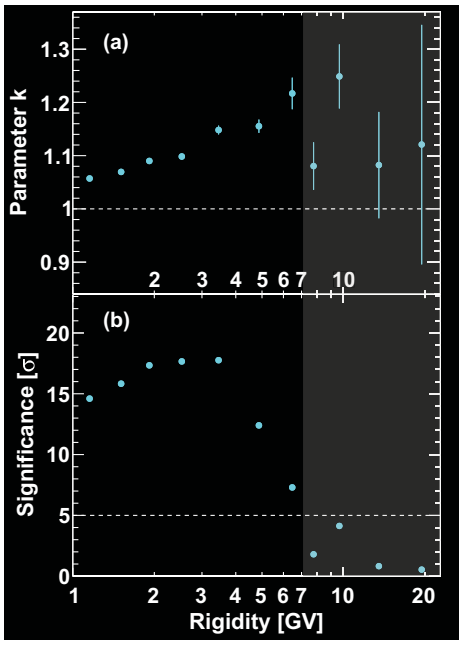

FIG. 4. (a) k parameter values obtained from the linear fits to the relative variation of the positron and proton fluxes as function of rigidity [see Eq. (2)] and (b) significance, in units of σ, of the deviation of the parameter k from unity as a function of rigidity. As seen, k gradually increases with rigidity and is significantly ($> 5\sigma$) greater than unity in the rigidity range from 1.00 to 7.09 GV, indicating that the positron flux is more modulated than the proton flux in this rigidity range.

bins from 1.00 to 5.90 GV. Figure 4(a) shows the results of the k^i as a function of rigidity. As seen, k^i gradually increases with rigidity from 1.055 ± 0.004 at the rigidity bin [1.00–1.33] GV to 1.20 ± 0.03 at the rigidity bin [5.90–7.09] GV. As shown in Fig. 4(b), k^i is greater than unity with a significance greater than 5σ for rigidities from 1.00 to 7.09 GV, indicating that the positron flux is more modulated than the proton flux in this rigidity range.

At a given rigidity below 7 GV, AMS observed that helium, which has a lower velocity than protons, is modulated more than protons [16]. In this Letter, we observe that, remarkably, positrons, which have a higher velocity, are also modulated more than protons. The contradiction in velocity dependence cannot be explained only by differences in the diffusive processes, since these are commonly accepted to be proportional to the velocity. Our simultaneous results on the velocity dependence of positrons, protons, and helium require a comprehensive model to consider other important effects, such as convection, adiabatic energy changes, and the shape of the flux rigidity dependence outside the heliosphere [38].

In conclusion, we presented the precision measurements of daily cosmic positron fluxes spanning 11 years over a rigidity range from 1.00 to 41.9 GV based on 3.4×10^6 positrons. The positron fluxes exhibit variations on multiple timescales. In the 11-year period, the positron fluxes show distinctly different time variations from the electron fluxes at short and long timescales. A hysteresis between the electron flux and the positron flux is observed with a significance greater than 5σ at rigidities below 8.5 GV, and significant structures in the electron-positron hysteresis are observed corresponding to sharp variations of both fluxes. On the contrary, positron and proton fluxes show nearly identical time variation. Remarkably, positron fluxes are modulated more than proton fluxes with a significance greater than 5σ for rigidities below 7 GV. These continuous daily positron fluxes, together with AMS daily electron, proton, and helium fluxes over an 11-year solar cycle, provide unique input to the understanding of both the charge-sign and mass dependencies of cosmic rays in the heliosphere.

We are grateful for important physics discussions with Igor Moskalenko and Subir Sarkar. We thank former NASA Administrator Daniel S. Goldin for his dedication to the legacy of the ISS as a scientific laboratory and his decision for NASA to fly AMS as a DOE payload. We also acknowledge the continuous support of the NASA leadership, particularly Kathryn Lueders and of the JSC and MSFC flight control teams that have allowed AMS to operate optimally on the ISS for over 12 years. We are grateful for the support of Glen Crawford of the DOE including resources from the National Energy Research Scientific Computing Center under Contract No. DE-AC02-05CH11231. We gratefully acknowledge the strong support from CERN including Fabiola Gianotti and the CERN IT department including Bernd Panzer-Steindel. We also acknowledge the continuous support from MIT and its School of Science, Nergis Mavalvala, and the Laboratory for Nuclear Science, Boleslaw Wyslouch. Research supported by: Chinese Academy of Sciences, Institute of High Energy Physics, Institute of Electrical Engineering, China Academy of Space Technology, National Natural Science Foundation (NSFC), and Ministry of Science and Technology, National Key R&D Program Grants No. 2022YFA1604802 and No. 2022YFA1604803, NSFC Grant No. 12275158, the China Scholarship Council, the provincial governments of Shandong, Jiangsu, Guangdong, Shandong University, and the Shandong Institute of Advanced Technology, China; the Academy of Finland, Project No. 321882, Finland; CNRS/IN2P3 and CNES, France; DLR under Grant No. 50OO1803 and computing support on the JARA Partition of the RWTH Aachen supercomputer, Germany; INFN and ASI under ASI-INFN Agreements No. 2019-19-HH.0, its amendments, No. 2021-43-HH.0, and ASI-University of Perugia Agreement No. 2019-2-HH.0, and the Italian Ministry of University and Research (MUR) through the program "*Dipartimenti di Eccellenza 2023–2027*" (Grant SUPER-C), Italy; the Consejo Nacional de Ciencia y Tecnología and UNAM, Mexico; NWO under Grant No. 680-1-004, Netherlands; FCT under Grant No. CERN/FIS-PAR/0013/2019, Portugal; CIEMAT, IAC, CDTI, and MCIN-AEI

under Grants No. PID2019–107988 GB-C21/C22 and No. CEX2019-000920-S, Spain; the Fondation Dr. Manfred Steuer, Switzerland; Academia Sinica, the National Science and Technology Council (NSTC), formerly the Ministry of Science and Technology (MOST), under Grants No. 111-2123-M-001-004 and No. 111-2112-M-006-029, High Education Sprout Project by the Ministry of Education at National Cheng Kung University, former Presidents of Academia Sinica Yuan-Tseh Lee and Chi-Huey Wong and former Ministers of NSTC (formerly MOST) Maw-Kuen Wu and Luo-Chuan Lee, Taiwan; the Turkish Energy, Nuclear and Mineral Research Agency (TENMAK) under Grant No. 2020TAEK(CERN)A5.H1.F5-26, Türkiye; and NSF Grant No. 2013228 and ANSWERS Proposals No. 2149809, No. 2149810, and No. 2149811, NASA Grant No. 80NSSC21K1392, USA, and LWS NASA Grant/Cooperative Agreement No. 80NSSC20K1819.

*Also at IRCCS Azienda Ospedaliero-Universitaria di Bologna, Bologna, Italy.

[1] M. S. Turner and F. Wilczek, Positron line radiation as a signature of particle dark matter in the halo, Phys. Rev. D **42**, 1001 (1990); J. Ellis, Particles and cosmology: Learning from cosmic rays, AIP Conf. Proc. **516**, 21 (2000); F. Donato, N. Fornengo, and P. Salati, Antideuterons as a signature of supersymmetric dark matter, Phys. Rev. D **62**, 043003 (2000); H. C. Cheng, J. L. Feng, and K. T. Matchev, Kaluza-Klein Dark Matter, Phys. Rev. Lett. **89**, 211301 (2002); M. Cirelli, R. Franceschini, and A. Strumia, Minimal dark matter predictions for galactic positrons, anti-protons, photons, Nucl. Phys. B **800**, 204 (2008); J. Kopp, Constraints on dark matter annihilation from AMS-02 results, Phys. Rev. D **88**, 076013 (2013); C. H. Chen, C. W. Chiang, and T. Nomura, Dark matter for excess of AMS-02 positrons and antiprotons, Phys. Lett. B **747**, 495 (2015); H. C. Cheng, W. C. Huang, X. Huang, I. Low, Y. L. Sming Tsai, and Q. Yuan, AMS-02 positron excess and indirect detection of three-body decaying dark matter, J. Cosmol. Astropart. Phys. 03 (2017) 041; Y. Bai, J. Berger, and S. Lu, Supersymmetric resonant dark matter: A thermal model for the AMS-02 positron excess, Phys. Rev. D **97**, 115012 (2018).

[2] P. D. Serpico, Astrophysical models for the origin of the positron "excess", Astropart. Phys. **39–40**, 2 (2012); T. Linden and S. Profumo, Probing the pulsar origin of the anomalous positron fraction with AMS-02 and atmospheric Cherenkov telescopes, Astrophys. J. **772**, 18 (2013); I. Cholis and D. Hooper, Dark matter and pulsar origins of the rising cosmic ray positron fraction in light of new data from the AMS, Phys. Rev. D **88**, 023013 (2013); D. Hooper, I. Cholis, T. Linden, and K. Fang, HAWC observations strongly favor pulsar interpretations of the cosmic-ray positron excess, Phys. Rev. D **96**, 103013 (2017); S. Profumo, J. Reynoso-Cordova, N. Kaaz, and M. Silverman, Lessons from HAWC pulsar wind nebulae observations: The diffusion constant is not a constant; pulsars remain the likeliest sources of the anomalous positron fraction; cosmic rays are trapped for long periods of time in pockets of inefficient diffusion, Phys. Rev. D **97**, 123008 (2018).

[3] P. Lipari, Interpretation of the cosmic ray positron and antiproton fluxes, Phys. Rev. D **95**, 063009 (2017); R. Cowsik, B. Burch, and T. Madziwa-Nussinov, The origin of the spectral intensities of cosmic-ray positrons, Astrophys. J. **786**, 124 (2014); K. Blum, B. Katz, and E. Waxman, AMS-02 Results Support the Secondary Origin of Cosmic Ray Positrons, Phys. Rev. Lett. **111**, 211101 (2013); P. Blasi, The Origin of the Positron Excess in Cosmic Rays, Phys. Rev. Lett. **103**, 051104 (2009).

[4] M. Aguilar *et al.*, First Result from the Alpha Magnetic Spectrometer on the International Space Station: Precision Measurement of the Positron Fraction in Primary Cosmic Rays of 0.5–350 GeV, Phys. Rev. Lett. **110**, 141102 (2013); High Statistics Measurement of the Positron Fraction in Primary Cosmic Rays of 0.5–500 GeV with the Alpha Magnetic Spectrometer on the International Space Station, Phys. Rev. Lett. **113**, 121101 (2014); Electron and Positron Fluxes in Primary Cosmic Rays Measured with the Alpha Magnetic Spectrometer on the International Space Station, Phys. Rev. Lett. **113**, 121102 (2014).

[5] M. Aguilar *et al.*, Towards Understanding the Origin of Cosmic-Ray Positrons, Phys. Rev. Lett. **122**, 041102 (2019).

[6] O. Adriani *et al.*, Cosmic-Ray Positron Energy Spectrum Measured by PAMELA, Phys. Rev. Lett. **111**, 081102 (2013); M. Ackermann *et al.*, Measurement of Separate Cosmic-Ray Electron and Positron Spectra with the Fermi Large Area Telescope, Phys. Rev. Lett. **108**, 011103 (2012); C. Grimani *et al.*, Measurements of the absolute energy spectra of cosmic-ray positrons and electrons above 7 GeV, Astron. Astrophys. **392**, 287 (2002); M. Boezio *et al.*, Measurements of cosmic-ray electrons and positrons by the Wizard/CAPRICE collaboration, Adv. Space Res. **27**, 669 (2001); M. Aguilar *et al.*, Cosmic-ray positron fraction measurement from 1 to 30 GeV with AMS-01, Phys. Lett. B **646**, 145 (2007); S. W. Barwick *et al.*, The energy spectra and relative abundances of electrons and positrons in the galactic cosmic radiation, Astrophys. J. **498**, 779 (1998); M. A. DuVernois *et al.*, Cosmic-ray electrons and positrons from 1 to 100 GeV: Measurements with HEAT and their interpretation, Astrophys. J. **559**, 296 (2001).

[7] A. W. Strong and I. V. Moskalenko, Propagation of cosmic-ray nucleons in the galaxy, Astrophys. J. **509**, 212 (1998); A. E. Vladimirov, S. W. Digel, G. Jóhannesson, P. F. Michelson, I. V. Moskalenko, P. L. Nolan, E. Orlando, T. A. Porter, and A. W. Strong, GALPROP WebRun: An internet-based service for calculating galactic cosmic ray propagation and associated photon emissions, Comput. Phys. Commun. **182**, 1156 (2011).

[8] C. Evoli, D. Gaggero, A. Vittino, G. Di Bernardo, M. Di Mauro, A. Ligorini, P. Ullio, and D. Grasso, Cosmic-ray propagation with DRAGON2: I. Numerical solver and astrophysical ingredients, J. Cosmol. Astropart. Phys. 02 (2017) 015.

[9] D. Maurin, F. Donato, R. Taillet, and P. Salati, Cosmic rays below $Z = 30$ in a diffusion model: New constraints on propagation parameters, Astrophys. J. **555**, 585 (2001).

[10] A. Putze, L. Derome, and D. Maurin, A Markov Chain Monte Carlo technique to sample transport and source

parameters of Galactic cosmic rays II. Results for the diffusion model combining B/C and radioactive nuclei, Astron. Astrophys. **516**, A66 (2010).
[11] M. S. Potgieter, Solar modulation of cosmic rays, Living Rev. Solar Phys. **10**, 3 (2013).
[12] M. S. Potgieter, The charge-sign dependent effect in the solar modulation of cosmic rays, Adv. Space Res. **53**, 1415 (2014).
[13] M. Aguilar *et al.*, Observation of Complex Time Structures in the Cosmic-Ray Electron and Positron Fluxes with the Alpha Magnetic Spectrometer on the International Space Station, Phys. Rev. Lett. **121**, 051102 (2018).
[14] M. Aguilar *et al.*, Temporal Structures in Electron Spectra and Charge Sign Effects in Galactic Cosmic Rays, Phys. Rev. Lett. **130**, 161001 (2023).
[15] M. Aguilar *et al.*, Periodicities in the Daily Proton Fluxes from 2011 to 2019 Measured by the Alpha Magnetic Spectrometer on the International Space Station from 1 to 100 GV, Phys. Rev. Lett. **127**, 271102 (2021). The new Φ_p data up to November 2021 will be published separately.
[16] M. Aguilar *et al.*, Properties of Daily Helium Fluxes, Phys. Rev. Lett. **128**, 231102 (2022). The new Φ_{He} data up to November 2021 will be published separately.
[17] O. Adriani *et al.*, Time Dependence of the Electron and Positron Components of the Cosmic Radiation Measured by the PAMELA Experiment between July 2006 and December 2015, Phys. Rev. Lett. **116**, 241105 (2016).
[18] X. Sun, J. T. Hoeksema, Y. Liu, and J. Zhao, On polar magnetic field reversal and surface flux transport during solar cycle 24, Astrophys. J. **798**, 114 (2015).
[19] M. Aguilar *et al.*, The Alpha Magnetic Spectrometer (AMS) on the International Space Station: Part II—Results from the first seven years, Phys. Rep. **894**, 1 (2021).
[20] A. Kounine, The alpha magnetic spectrometer on the international space station, Int. J. Mod. Phys. E **21**, 1230005 (2012); S. Ting, The alpha magnetic spectrometer on the International Space Station, Nucl. Phys. B, Proc. Suppl. **243–244**, 12 (2013); B. Bertucci, The AMS-02 detector operation in space, Proc. Sci. EPS-HEP2011 (**2011**) 67; M. Incagli, Astroparticle physics with AMS02, AIP Conf. Proc. **1223**, 43 (2010); R. Battiston, The antimatter spectrometer (AMS-02): A particle physics detector in space, Nucl. Instrum. Methods Phys. Res., Sect. A **588**, 227 (2008).
[21] See Supplemental Material at http://link.aps.org/supplemental/10.1103/PhysRevLett.131.151002 for the AMS detector description, details of event selection, definition of years, details of wavelet analysis, hysteresis analysis, figures, and the tabulated daily positron fluxes as functions of rigidity.
[22] K. Lübelsmeyer *et al.*, Upgrade of the alpha magnetic spectrometer (AMS-02) for long term operation on the International Space Station (ISS), Nucl. Instrum. Methods Phys. Res., Sect. A **654**, 639 (2011).
[23] B. Alpat *et al.*, The internal alignment and position resolution of the AMS-02 silicon tracker determined with cosmic-ray muons, Nucl. Instrum. Methods Phys. Res., Sect. A **613**, 207 (2010).
[24] G. Ambrosi, V. Choutko, C. Delgado, A. Oliva, Q. Yan, and Y. Li, The spatial resolution of the silicon tracker of the Alpha Magnetic Spectrometer, Nucl. Instrum. Methods Phys. Res., Sect. A **869**, 29 (2017).
[25] Y. Jia, Q. Yan, V. Choutko, H. Liu, and A. Oliva, Nuclei charge measurement by the Alpha Magnetic Spectrometer silicon tracker, Nucl. Instrum. Methods Phys. Res., Sect. A **972**, 164169 (2020).
[26] F. Hauler *et al.*, The AMS-02 TRD for the International Space Station, IEEE Trans. Nucl. Sci. **51**, 1365 (2004); Ph. Doetinchem *et al.*, Performance of the AMS-02 transition radiation detector, Nucl. Instrum. Methods Phys. Res., Sect. A **558**, 526 (2006); Th. Kirn, The AMS-02 TRD on the International Space Station, Nucl. Instrum. Methods Phys. Res., Sect. A **706**, 43 (2013).
[27] V. Bindi *et al.*, Calibration and performance of the AMS-02 time of flight detector in space, Nucl. Instrum. Methods Phys. Res., Sect. A **743**, 22 (2014).
[28] C. Adloff *et al.*, The AMS-02 lead-scintillating fibres electromagnetic calorimeter, Nucl. Instrum. Methods Phys. Res., Sect. A **714**, 147 (2013).
[29] A. Kounine, Z. Weng, W. Xu, and C. Zhang, Precision measurement of 0.5 GeV–3 TeV electrons and positrons using the AMS electromagnetic calorimeter, Nucl. Instrum. Methods Phys. Res., Sect. A **869**, 110 (2017).
[30] J. Allison *et al.*, Recent developments in GEANT4, Nucl. Instrum. Methods Phys. Res., Sect. A **835**, 186 (2016); GEANT4 developments and applications, IEEE Trans. Nucl. Sci. **53**, 270 (2006); S. Agostinelli *et al.*, GEANT4–a simulation toolkit, Nucl. Instrum. Methods Phys. Res., Sect. A **506**, 250 (2003).
[31] M. Aguilar *et al.* (AMS Collaboration), Measurement of the geomagnetic cutoff with the Alpha Magnetic Spectrometer on the International Space Station (to be published).
[32] C. C. Finlay *et al.*, International Geomagnetic Reference Field: The eleventh generation, Geophys. J. Int. **183**, 1216 (2010); E. Thébault *et al.*, International Geomagnetic Reference Field: The 12th generation, Earth Planets Space **67**, 79 (2015); Geomagnetic Field Modeling Working Group, IGRF-13 model (2019), https://www.ngdc.noaa.gov/IAGA/vmod/igrf.html.
[33] P. Bobik, G. Boella, M. J. Boschini, D. Grandi, M. Gervasi, K. Kudela, S. Pensotti, and P. G. Rancoita, Magnetospheric transmission function approach to disentangle primary from secondary cosmic ray fluxes in the penumbra region, J. Geophys. Res. **111**, A05205 (2006); N. A. Tsyganenko and M. I. Sitnov, Modeling the dynamics of the inner magnetosphere during strong geomagnetic storms, J. Geophys. Res. **110**, A03208 (2005).
[34] M. Aguilar *et al.*, Precision Measurement of the Proton Flux in Primary Cosmic Rays from Rigidity 1 GV to 1.8 TV with the Alpha Magnetic Spectrometer on the International Space Station, Phys. Rev. Lett. **114**, 171103 (2015).
[35] Note that the data can also be downloaded in different formats from the AMS Web site https://ams02.space/sites/default/files/publication/202307/table-s1-s3268.csv, the ASI cosmic-ray database at https://tools.ssdc.asi.it/CosmicRays, and the LPSC cosmic-ray database at https://lpsc.in2p3.fr/crdb/.
[36] C. Torrence and G. P. Compo, A practical guide to wavelet analysis, Bull. Am. Meteorol. Soc. **79**, 61 (1998).
[37] I. Richardson and H. Cane, Near-Earth Interplanetary Coronal Mass Ejections since January 1996; see

https://izw1.caltech.edu/ACE/ASC/DATA/level3/icmetable2.htm, specifically the events starting from March 16, 2015 and from July 16, 2017.

[38] L. J. Gleeson and W. I. Axford, Cosmic rays in the interplanetary medium, Astrophys. J. **149**, L115 (1967); L. J. Gleeson and W. I. Axford, Solar modulation of galactic cosmic rays, Astrophys. J. **154**, 1011 (1968); L. J. Gleeson and W. I. Axford, The compton-getting effect, Astrophys. Space Sci. **2**, 431 (1968); J. R. Jokipii and E. N. Parker, On the convection, diffusion, and adiabatic deceleration of cosmic rays in the solar wind, Astrophys. J. **160**, 735 (1970); L. J. Gleeson and G. M. Webb, Energy changes of cosmic rays in the interplanetary region, Astrophys. Space Sci. **58**, 21 (1978); G. M. Webb and L. J. Gleeson, On the equation of transport for cosmic-ray particles in the interplanetary region, Astrophys. Space Sci. **60**, 335 (1979); M. S. Potgieter and H. Moraal, A drift model for the modulation of galactic cosmic rays, Astrophys. J. **294**, 425 (1985); I. G. Richardson, Energetic particles and corotating interaction regions in the solar wind, Space Sci. Rev. **111**, 267 (2004); H. Moraal, Cosmic-ray modulation equations, Space Sci. Rev. **176**, 299 (2013).